Chapter 4

Ionized Carbon towards Cas A

4.1 Introduction

The interstellar medium in the direction of the strong radio source Cas A has been extensively studied in radio recombination lines of carbon. Konovalenko and Sodin (1980) were the first to observe a low frequency (26.3 MHz) absorption line towards Cas A which was later correctly identified as the 630α recombination line of carbon by Blake, Crutcher & Watson (1980). Since then, this direction has been studied in many transitions in carbon with principal quantum numbers ranging from n=766 to n=166, which correspond to frequencies ranging from 14 MHz to 1400 MHz respectively (Payne, Anantharamaiah & Erickson 1989, 1994 and references therein).

In their observations of carbon recombination lines towards Cas A in the frequency range 34 – 325 MHz, Payne, Anantharamaiah & Erickson (1989, hereafter PAE89) detected a smooth transition from absorption to emission with increasing frequency; the lines are in emission at frequencies above 200 MHz and in absorption below 115 MHz. At frequencies where lines are seen in emission, the line widths are essentially due to Doppler broadening and the carbon line spectrum is resolved into three components at velocities near –1 $\mathrm{kms^{-1}}$, –37 $\mathrm{kms^{-1}}$ and –48 $\mathrm{kms^{-1}}$. These velocities correspond to the Orion and Perseus arms in this direction. However, at lower frequencies where the lines appear in absorption, the Perseus arm components at –37 $\mathrm{kms^{-1}}$ and –48 $\mathrm{kms^{-1}}$ blend into a single feature because of pressure and radiation broadening, both of which are strong functions of the principal quantum number n. This broadening results in Voigt profiles which have a narrow Gaussian-like shape in the central region (due to Doppler broadening) and broad Lorentzian wings. Observationally it has been difficult to detect the Lorentzian wings in the low frequency recombination lines due to practical problems such as weakness of the line and baseline removal from the observed spectrum. The procedures that are generally used for baseline removal may reduce the amplitude of the Lorentzian wings thus leading to wrong values of line widths and line strengths. Sorochenko and Smirnov (1990) noted that the reported widths and strengths of the low frequency lines were based on Gaussian profiles instead of Voigt profiles and they applied corrections to the integrated optical depths ($\int \tau d\nu$) by assuming the latter. More recently, Payne, Anantharamaiah & Erickson (1994, hereafter PAE94) have quantitatively shown that baseline-removal procedure has indeed led to an underestimation of both the line strength and the line width. They constructed model line profiles using probable cloud parameters and showed that at the lowest frequencies, the integrated optical depths of the observed lines could have been underestimated by a factor of almost 3 due to baseline removal. At higher frequencies, the observed profiles matched well with their model profiles.

For most of the last 16 years since the low frequency carbon recombination lines were first detected towards Cas A, two types of models have been debated over: 1) the warm gas model with electron temperature T_e in the range 35 – 75K and electron density n_e in the range 0.05 - 0.1 cm^{-3} which could be coexistent with the HI phase of the ISM (Walmsley & Watson 1982, PAE89, PAE94) and 2) the cold gas model with $T_e \sim 16 - 20$ K and $n_e \sim 0.3$ cm^{-3} (Ershov et. *al.*, 1984, 1987, Sorochenko 1996) which could be coexisting with the molecular hydrogen component of the ISM. Ershov et. *al.* (1984,1987) showed that the cold gas model explained their observations better than the warm gas model and suggested that the carbon recombination lines could originate in small (≤ 1 pc), dense ($n_H = 10^3 - 10^4$ cm^{-3}) clouds where the main agent for ionizing carbon would be diffuse ultraviolet radiation.

More recently, however, PAE94 have provided evidence that show strong support for the warm gas model. Based on data spanning almost two decades in frequency, PAE94 have developed a model which satisfactorily explains the observed variation of integrated optical depth with principal quantum number. The parameters of their model provide thermal balance in the clouds and pressure equilibrium with the environment. In this model, PAE94 have considered a new boundary condition ($b_n \rightarrow 0$ as $n \rightarrow \infty$) suggested by Gulyaev and Nefedov (1989, hereafter GN89) for calculating the departure coefficients b_n, and also included the occupation probabilities of high quantum number levels, which are affected by the presence of electrons and neutral particles in the cloud (Hummer and Mihalas 1988, hereafter HM88). The one parameter that the model by PAE94 is unable to explain is the widths of the lines which is better explained by earlier models which used the boundary condition of $b_n \rightarrow 1$ as $n \rightarrow \infty$ and had dielectronic-like recombination effects (Watson, Western & Christensen 1980, Walmsley & Watson 1982) included in the calculation of b_n. However, the earlier models do not provide thermal balance and are out of pressure equilibrium although they do explain the observed variation in the integrated optical depth and line width with quantum number.

In this Chapter, we use our different observations towards Cas A, presented in Chapter 3, together with other available data to obtain constraints on the properties of the line forming regions.

4.2 Observations towards Cas A

Our observations towards Cas A are summarized below:

(1) The carbon recombination line near **34.5** MHz observed towards Cas A with the Gauribidanur Array resulted in a high signal to noise ratio spectrum, which, after removal of a simple linear baseline, clearly shows a Voigt profile with distinct Lorentzian wings as expected. This profile leads to a reliable estimate of the integrated optical depth at a low frequency where the line width is dominated by pressure or radiation broadening. The integrated line strength is used in modelling the line region. The parameters of the Voigt profile provide constraints on the electron density, temperature and radiation background in the cloud. The observed spectrum near **34.5** MHz is shown in Fig **4.1(a).** The spectrum is hanning smoothed and therefore has a resolution of **0.5** kHz. A single-component Voigt profile fit to the **34.5** MHz profile is also shown in Fig **4.1(a).** The fitted parameters are listed in **Table 4.1.**

Table **4.1 Line fit Parameters**

	ν MHz	Cnα	T_l/T_c 10^{-3}	V_{lsr} kms^{-1}	ΔV_D kms^{-1}	ΔV_L kms^{-1}	$\int \tau d\nu$ s^{-1}
1	34.5	C575α	-3.7 ± 0.2	-42.0 ± 0.2	5.0 ± 0.6	26.0 ± 3.1	16.6 ± 0.5
2	327	C272α	1.2 ± 0.1	-43.0 ± 0.1	5.0 ± 0.5	-	-7.0 ± 0.5

(2) The carbon recombination line observations near 327 MHz made using the Ooty Radio Telescope showed a narrow profile whose line width is essentially due to Doppler broadening. The detected line is in emission. As pointed out by PAE89, the detection of an emission line from relatively cold clouds (T $\sim$ **100 K**) against a strong background source ($T_B \sim 10^5$ K) is direct evidence for stimulated emission due to inverted population of the high quantum number states in carbon. The emission line near 327 MHz is

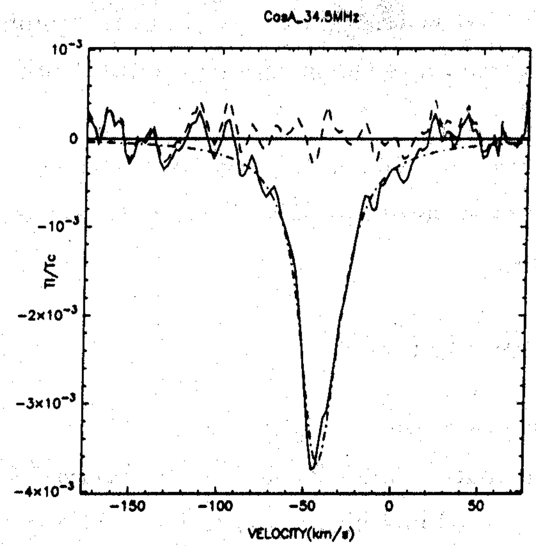

Figure 4.1 (a) **Spectrum towards Cas A at 34.5 MHz. The solid line shows the observed spectrum, the dash-dotted line shows the Voigt profile fitted to the absorption line and the dashed line shows the residuals. The fit parameters are $T_l/T_{sys} = -3.7(0.1)$ x 10^{-3}, radial velocity is $-42(0.3)$ kms^{-1}, Doppler width is 5(0.3) kms^{-1}and Lorentzian width is 26(0.6) kms^{-1}.**

used to obtain the Doppler width and together with other data is used to constrain the models of the line emitting region. The observed spectrum near 327 MHz is shown in Fig 4.1. A Gaussian profile fitted to the emission line is also shown in Fig 4.1(b) and the fitted parameters are listed in Table 4.1 .

(3) The spatial distribution of the C270α emission line near 332 MHz over the face of Cas A was obtained using the Very Large Array in USA. The spatial distribution of ^{12}CO emission near 115 GHz, which traces the molecular gas over the face of Cas A, was obtained using the 10.4 m millimeter wave telescope of RRI at Bangalore. These two distributions and also that of neutral HI obtained from published 21 cm data are compared to distinguish between the possible association of the ionised carbon region with molecular or atomic gas in the ISM.

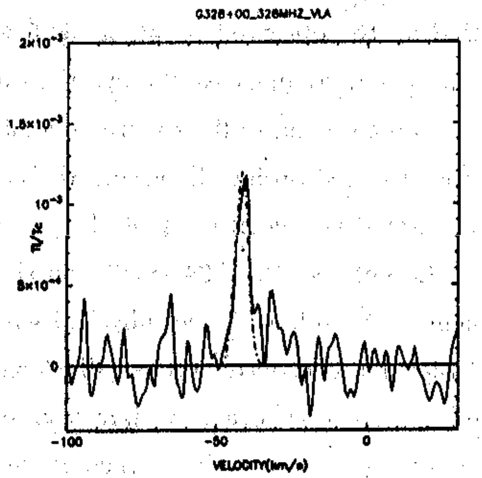

Figure 4.1 (b) **Spectrum towards Cas A at 328 MHz. The solid line shows the observed spectrum, the dash-dotted line shows the Gaussian profile fitted to the absorption line and the dashed line shows the residuals. The fit parameters are $T_l/T_{sys.}$ = 1.2 × 10^{-3}, radial velocity is –47.5 kms^{-1} and width is 5 kms^{-1}.**

4.3 Properties of the Line Forming Region

4.3.1 Physical limits from Observed Line Width

The carbon recombination line towards Cas A appears in absorption at 34.5 MHz and in emission near 327 MHz as shown in Fig 4.1. As can be seen in this Fig, there is a dramatic difference in the line width at the two frequencies. It is clear that pressure and/or radiation broadening, both of which are strong functions of frequency, is responsible for the large line width at 34.5 MHz. The higher frequency line is broadened essentially by thermal or turbulent motions in the cloud. While the measured width of the lower frequency line can be used to constrain the electron density in the clouds, the higher frequency observations would be useful to obtain limits on the temperature and to constrain possible association with HI or molecular clouds.

Although earlier observations towards Cas A have shown that the carbon recombination lines near 337 MHz may have three components (near –48, –39 and –1 kms^{-1}) (Anantharamaiah *et.al.*, 1994), similar to the hydrogen 21-cm line and the molecular lines, the present study at 327 MHz has detected only the strong Perseus arm component at a V_{lsr} of –48 kms^{-1}. The detection of only the strongest component in Fig 4.1(b) is probably due to the relatively low signal to noise ratio of the spectrum. In Fig 4.1(b), a model Gaussian profile with a full width at half maximum of 5 kms^{-1} is shown superposed on the observed profile. The best-fitting Gaussian parameters are listed in Table 4.1. The observed width of 5 kms^{-1} of the C272α lines gives a not too significant upper limit of 6500K for the temperature of the cloud.

In Fig 4.1(a), a Voigt profile with a Doppler width of 5 kms^{-1} and Lorentz width of 26 kms^{-1} has been superposed on the observed profile at 34.5 MHz with other fit parameters as listed in Table 4.1. At low-frequencies, the two Perseus arm components merge into a single feature due to pressure and radiation broadening and hence a single Voigt component was fitted to the observed profile. However, we found that it is in fact possible to fit two components centered at velocities of –44 kms^{-1} and –38 kms^{-1} with Doppler widths of 5 kms^{-1} each, Lorentz width of 24 kms^{-1} and the optical depths in the ratio 3:1. The two component fit is probably more physical when we consider the high-frequency RRL, HI and molecular line observations, all of which show the two components. A closer inspection of Fig 4.1(a) reveals a slight asymmetry in the profile near 0 kms^{-1} which could probably be due to the Orion arm component. The low signal to noise ratio of this component made the fit unstable when we attempted fitting three Voigt profiles to the observed spectrum. We use the parameters derived from a single component fit for consistency with earlier modelling (*e.g.* PAE94), and also because the Lorentz width is nearly the same when either one or two components are fitted to the spectrum.

It is clear that the Voigt profile obtained for the carbon recombination line near 34.5 MHz (Fig 4.1(a)) is due to either radiation broadening or pressure broadening or more likely due to a combination of both. If the entire Lorentzian width of 26 kms^{-1} is assumed to be due to radiation broadening, then, using the formula from Shaver (1975), we get an upper limit of 7700 K for the radiation temperature at 100 MHz (T_{R100}) as seen by the cloud. Since the galactic non-thermal background in this directioe has $T_{R100} \sim 800$ K, the major contribution to the radiation temperature, in this case, should come from Cas A itself. The implied radiation temperature gives a lower limit of 50 pc for the distance of the aloud from Cas A, assuming the distance to Caa A to be 3.4 kpc, the linear size of Cas A to be 5 pc and the flux density of Cas A at 100 MHz to be 12300 Jy (Baars *et al.*, 1977).

Pressure broadening depends directly on the electron density and it is also a weak function of electron temperature ($\propto T_e^{-0.1}$). If the cloud is far away from Cas A and therefore subjected to only the galactic non-thermal background radiation (*i.e.* T_{R100} = 800 K), then for an electron temperature of 75 K, which is typical of HI clouds, the observed Lorentzian width of 26 kms^{-1} implies an electron density of 0.16 cm^{-3}. If the temperature is as low as 20 K, which is typical of molecular clouds, then the implied electron density is 0.68 cm^{-3}. On the otherhand, if the radiation temperature is

Table 4.2 Parameters constrained from line width

T_e K	T_{R100} K	n_e cm^{-3}	n_H T_e cm^{-3} K
75	800	0.16	4×10^4
	1600	0.12	3×10^4
	3200	0.03	7500
20	800	0.68	4.5×10^4
	1600	0.49	3.3×10^4
	3200	0.11	7330

These models assume $\delta_C \sim 1.0$.

four times the galactic background (*i.e.* T_{R100} = 3200 K), then the electron density is 0.03 cm^{-3} for T_e = 75 K and 0.11 cm^{-3} for T_e = 20 K. It is clear that, from the observed Lorentzian width, it is possible to obtain constraints only on the combination of electron density, temperature, and the radiation background. In Table 4.2, for T_e = 75 K and 20 K, values of electron densities are given for three different values of radiation temperature T_{R100}. In Fig 4.2, we show the variation of the observed line width with quantum number and the model (solid line) based on the combination of parameters given in Table 4.2. All the models given in Table 4.2, which are obtained from the observed line width at 34.5 MHz, predict almost identical variation of linewidth with quantum number. It appears from Fig 4.2, that all the observations beyond n=600 may have underestimated the line width.

If all the electrons in the cloud come from ionization of carbon (*i.e.* $n_e = n_C$) and if we assume a value for the abundance of carbon ($[n_C/n_H]$) and its depletion factor (δ_C), then we can obtain an estimate of the thermal pressure in the cloud using

$$n_H T = \frac{n_e}{\delta_C [n_C/n_H]} T_e.$$

Column 4 of Table 4.2 gives the values of $n_H T$ obtained using δ_C = 1 (*i.e.* no depletion of carbon) and $[n_C/n_H]$ = 3 x 10^{-4} (*i.e.* interstellar abundance). If the depletion is increased by some factor theh the thermal pressure also increases by the same factor. The implied thermal pressure is high in all the models. Only models with high radiation temperature and no depletion give estimates which are closer to, but still higher than the interstellar pressure which ranges between 3000 – 5000 K cm^{-3} (McKee

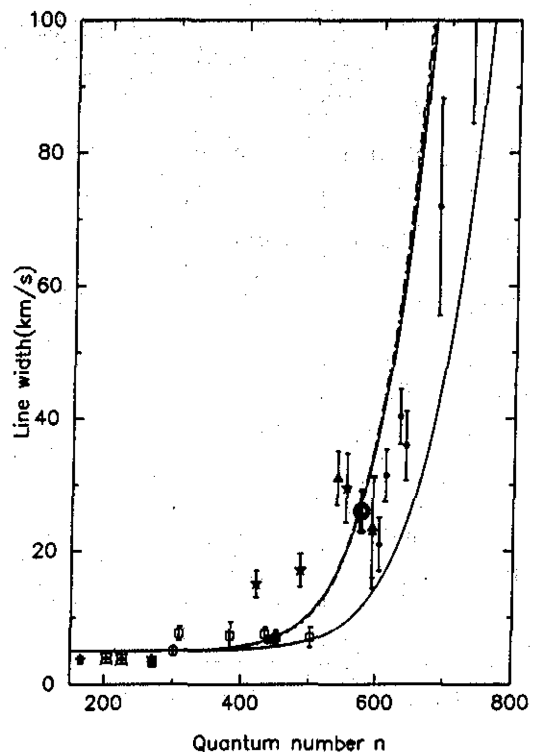

Figure 4.2 The observed variation in line width with quantum number is plotted here as data points. Our data point at 34.5 MHz is shown as a bold circle. The curves show the expected variation for different combinations of T_{R100} , T_e & n, for a Doppler line width of 5 kms^{-1}. The curves for T_e = 75 K and combinations of T_{R100} = 800 K, n_e = 0.16 cm^{-3} ; T_{R100} = 1600 K, n_e = 0.12 cm^{-3} ; T_{R100} = 3200 K, n_e = 0.03 cm^{-3} and for T_e = 20 K, T_{R100} = 800 K, n_e = 0.68 cm^{-3} ; T_{R100} = 3200 K, n_e = 0.11 cm^{-3} trace almost similar curves as shown in the figure. The single solid curve is for T_{R100} = 800 K, T_e = 35 K & n, = 0.05 cm^{-3} .

and Ostriker 1977, Kulkarni and Heiles 1988). It is possible that these clouds are not in pressure equilibrium with the ISM.

4.3.2 Spatial Distributions of C270α, ^{12}CO and H I lines

It is clear from the discussion above that, based on the width of the low-frequency recombination lines, the ioniaed carbon regions could be associated with either the cold ($T_e \sim$ 20 K) molecular clouds in the direction of Cas A or the warmer ($T_e \sim$ 100K) atomic H I clouds. In order to get a further constraint on the possible association, we compare the spatial distribution of ionized carbon regions obtained over the face of Cas A from VLA observations of the C270α line with that of ^{12}CO and 21 cm H I line.

In Fig 4.3 (a), we show the distribution of optical depth of the C270α line over the face of Cas A with a resolution of 1′ at four different radial velocities. These Yelocities correspond to the strong Perseus arm component hear − 47 kms^{-1}. The width of each channel is 1.3 kms^{-1}. The largest optical depths are in the channel with a radial velocity of -46.6 kms^{-1}. There is a gradient in the optical depth from east to west with the strongest optical depths at the western boundary. A secondary peak appears near the centre in this velocity channel. In the channel with a centre velocity of -45.3 kms^{-1}, there is a sharp gradient in the optical depth from north-east to south-west. At the other two velocities (−48.0 $kms^{-1}$and −49.4 kms^{-1}), the peak optical depth is near the centre of Caa A.

For comparison, the ^{12}CO emission over the face of Cas A with the same resolution (*i.e.* 1′) is shown in Fig 4.3 (b). It is clear from Figs 4.3 (a) and 43 (b) that the distribution of ^{12}CO and C270α lines are very different. For example hardly any molecular emission is seen at a velocity of –49.3 kms^{-1}whereas the same channel in C270α line shows considerable emission. At –46.7 kms–'and –48 kms^{-1}, the ^{12}CO emission has a strong concentration in the south-east region which is not seen in the recombination line. We therefore conclude that the spatial structure of carbon recombination lines towards Cas A has very little similarity with the structure of molecular gas in that direction.

On the otherhand, there is reasonable correspondence between the spatial distribution of the optical depths of the C270α recombination line and the 21 cm *H I* absorption line towards Caa A. Fig 4, taken from Anantharamaiah *et.al.* (1994), shows the spatial distribution of the optical depths of C270α and H I line and ^{12}CO emission over four velocity ranges. Correspondence between C270α and H I is particularly evident in two velocity ranges viz., –45.3 to 46.6 $kms^{-1}$and −49.4 to −50.8 kms^{-1}. In these two velocity ranges, the position of the peaks and the dinection of the gradient in the optical depths are very similar in C270α and *H I* maps. On the otherhand, in these same velocity ranges the ^{12}CO distribution is completely different and in fact there is hardly any ^{12}CO emission in the lower velocity range. There is however aome similarity between all the three distributions, *i.e.* C270α, *Hi* and ^{12}CO , 'in the velocity range –35.6 to –39.8 kms^{-1}.

On the whole it does appear that the spatial distribution'of C270α over the face of Cas A has better correspondence with that of H I distribution than with the distribution of ^{12}CO . This comparison thus favours the association of the carbon line region with the neutral H I component.

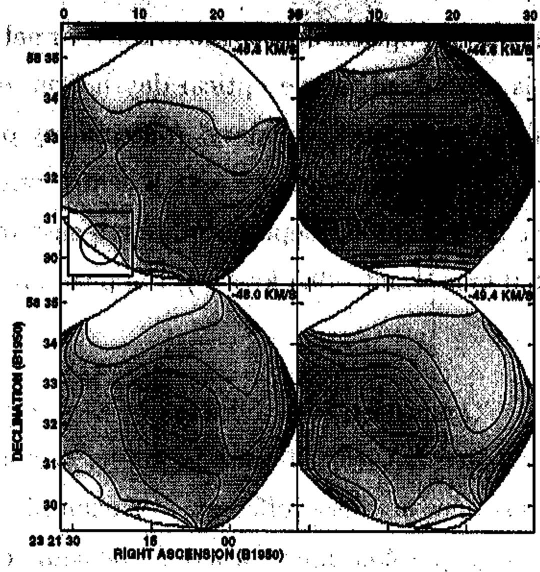

Figure 4.3 (a) Variation in observed C270α optical depth across Cas A at different radial velocities is shown here. The grey scale flux varies from 0 to 0.03. The contour levels are 1,2,3,4,5,7,9,11 in units of 0.001. The radial velocity is noted in the top right corner of each panel.

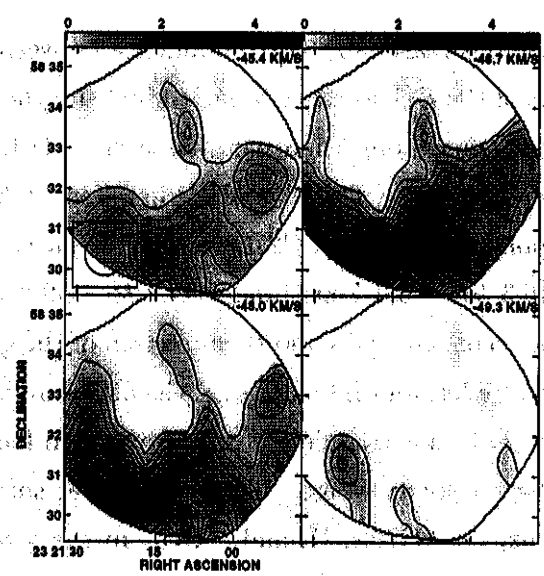

Figure 4.3 (b) Variation in observed ^{12}CO emission across Cas A at different radial velocities is shown here. The grey scale flux ranges from 0 to 5 K. The contour levels are 1,2,3,4,5,6,7,8,9, 10,11,13,15 in units of 0.3 K.

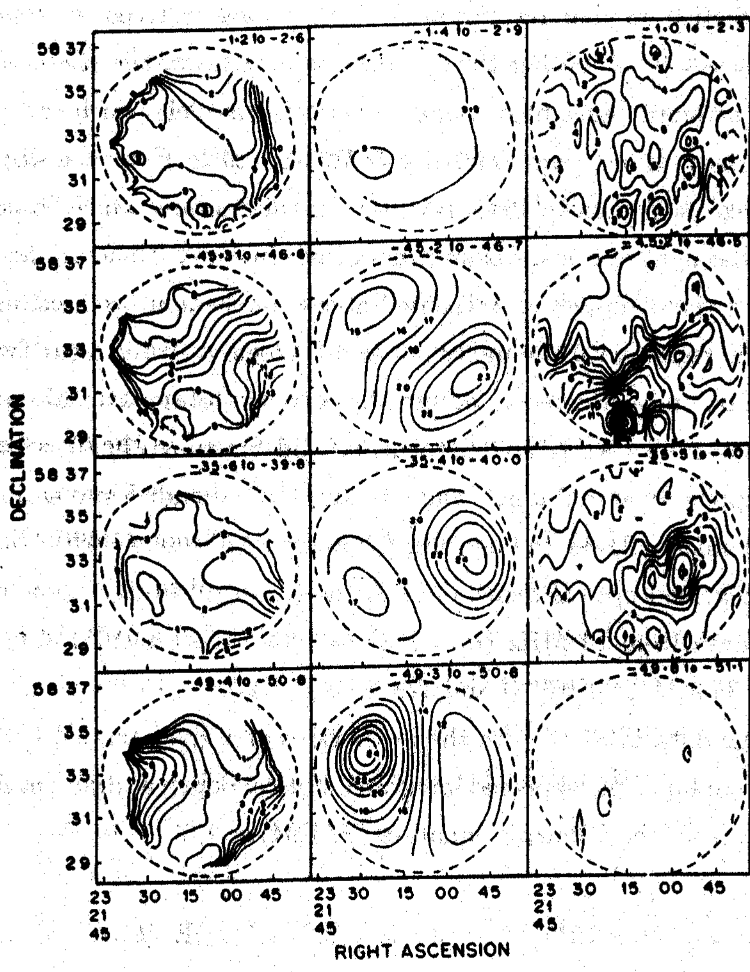

Figure 4.4 Distribution of C270α, H I and ^{12}CO emission over the face of Cas A over four velocity ranges (from Anantharamaiah *et.al.* 1994). Conaour levels are 1 unit $= 2 \times 10^{-4}$ for C270α, 0.1 for H I, and 0.3 K for ^{12}CO.

4.3.3 Constraints from the Integrated Line Strength

Carbon recombination lines towards Cas A has been observed over almost two decades in frequency - 14 MHz to 1400 MHz (Konovalenko 1990, PAE89 and Sorochenko & Walmsley 1991). The direction of Cas A has the special advantage that, although the above observations have been made with widely varying beamwidths, a direct comparison of all the measurements can be made. This comparison is possible since the continuum emission from Cas A, against which the lines are detected, overwhelms the total system temperature at all these frequencies even for moderate size telescopes. Therefore the effective angular resolution of all these observations corresponds to the angular size of Cas A ($\sim$ 5') rather than to the beamwidths of the telescopes used.

A number of attempts have been made to construct models which could satisfactorily explain the observations (*e.g.* Walmsley & Watson 1982, Ershov *et.al.* 1984, 1987, PAE89, Sorochenko & Walmsley 1991, PAE94). In this section, we reexamine some of these models in the light of our measurements of the integrated optical depths at 34.5 and 327 MHz and the comparison, presented above, of the spatial distribution of the recombination line region with the molecular and H I regions in the direction of Cas A. To combine with our measurements, we use the corrected observational data at other frequencies tabulated by PAE94 and Sorochenko and Smirnov (1990). Since the two Perseus arm components at –39 kms^{-1} and -47 kms^{-1} are blended into a single feature due to line broadening at lower frequencies, following PAE89 and PAE94, we consider only the total integrated optical depth of both the features. In Fig 5, we have shown all the available data from 14 MHz (n = 768) to 1400 MHz (n=165) along with our measurements at 34.5 MHz (n=578) and 328 MHz (n=270).

To compare the data in Fig 5 with the predictions of a given model, specified by a combination of T_e and n_e, the expected integrated optical depth at different frequencies ν can be obtained from the following equation (PAE94)

$$\int \tau_\nu d\nu = 2.046 \times 10^6 T_e^{-5/2} \exp(1.58 \times 10^5/(n^2 T_e)) \mathrm{EM} b_n \beta_n \quad s^{-1} \tag{4.1}$$

where EM is the emission measure defined as $n_e n_{C^+} l$, l is the path length through the cloud, and b_n and β_n are the coefficients related to the departure of the level populations from LTE values. Modelling proceeds by' first selecting a combination of T_e and n_e and an appropriate background radiation temperature T_{R100} which is consistent with the observed line width at 34.5 MHz as shown for example in Table 4.2. The departure coefficient b_n and its derivative β_n are computed for the selected combination of T_e , n_e and T_{R100} using the computer code first developed by Salem

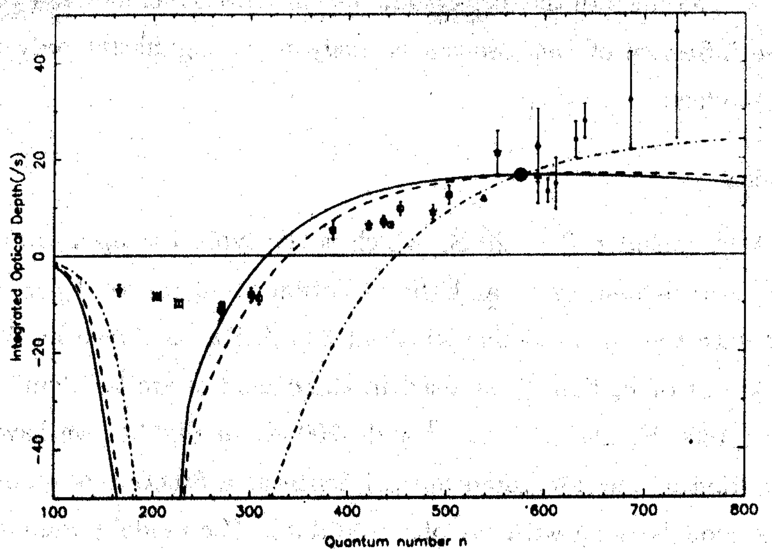

Figure 4.5 **Low temperature models - Solid line is for $T_e = 20$ K, $n_e = 0.68$ cm^{-3} &T_{R100} = 800 K; the dashed line is for $T_e = 20$ K, $n_e = 0.49$ cm^{-3} & $T_{R100} = 1600$ K; the dash-dots;& line is for $T_e = 20$ K, $n_e = 0.11$ cm^{-3} & $T_{R100} = 3200$ K. The influence of dielectronic-like recombination process on the level populations has been included in these models. The data obtained by us at 34.5 MHz is shown by a bold-filled circle.**

and **Brocklehurst** *(1979)*. **This** code was modified later by Walmsley & Watson *(1982)* to include the effects of a **dielectronic-like** recombination process in carbon suggested by Watson, **Western** and **Christensen** *(1980)*. The **code** was further modified by **PAE94** to include the choice of an alternate boundary condition suggested by Gulyaev and **Nefedov** (1989) **and** to **calculate** the **departure** coefficientsup to large quantum numbers $(n \sim 10000)$. **The unknown** emission measure, EM, in **Eqn** 4.1 **above** is obtained by using the **measured** value of $\int \tau_\nu d\nu$ at 34.5 MHz.

Another **physical** quantity, **the depletion** factor of carbon, δ_c, enters the calculation indirectly. In considering the effect of the dielectronic-like process in carbon, the departure coefficients b_n and β_n depend **on the** relative population of the fine structure states $^2P_{1/2}$ and $^2P_{3/2}$ in carbon, which are involved in the process (**Watson,** Western and **Christensen** *1980,* **Walmsley** & Watson *1982,* **Ponomarev** and Sorochenko *1992,* **PAE94**). In turn, the **relative** population of $^2P_{1/2}$ and $^2P_{3/2}$ states depend on the density **of electrons** (n_e) and the density of **neutral atoms** (n_H). If we **assume** that all the electrons in the **cloud** are **from ionization of** carbon, then the neutral density is given by $n_H = \frac{n_e}{\delta_C[n_C/n_H]}$, where $[n_C/n_H] = 3 \times 10^{-4}$ is the cosmic abundance of carbon.

Using the modelling procedure outlined above, we now examine the two types of models *i.e.* the cold gas model and the warm gas model, for the carbon line regions towards Cas A. The effect of the dielectronic-like process is included in both the models, although, the influence of this process is likely to be significant only in the higher temperature models.

Cold Gas Models

In this model we consider $T_e = 20\ K$, which is the typical temperature in molecular clouds. The electron density n_e and the radiation temperature T_{R100} are chosen to be consistent with the observed line width at 34.5 MHz, as shown in Table 4.2. The three combinations of n_e and T_{R100} used in these models are 0.68 cm^{-3} and 800 K, 0.49 cm^{-3} and 1600 K, and 0.11 cm^{-3} and 3200 K. In Fig 4.5, we have plotted the predicted variation of the integrated optical depth as a function of quantum number for these three models along with the observed data. The model parameters are given in Table 4.3. As seen in Table 4.3, for electron densities of 0.68 cm^{-3} and 0.49 cm^{-3}, the pathlength through the gas is 0.03 and 0.07 pc respectively. These pathlengths are very small compared to the lateral extent of the cloud, which is at least as large as that of Cas A (see Fig 4.3 (a)), *i.e.* > 5 pc. These models thus imply a sheet like geometry for the line forming regions. Such a geometry may be reasonable if the carbon lines are formed in thin outer layers of molecular clouds as suggested by Sorochenko & Walmsley (1991). In such a case, however, the spatial distribution of the carbon line emission over the face of Cas A should show correspondence with, the distribution of molecular gas. As shown in the previous Section such a correspondence is not seen. It is also clear from Fig 4.5 that none of the cold gas models provide a good fit to the observed data. All the three models predict very large optical depths near $n \sim 200$ which is not observed. While two of the models correctly predict the frequency of turnover from absorption to emission, neither of these models account for the observed line strengths at higher quantum numbers. In view of these difficulties, we do not favour the cold gas gas models in which the carbon line forming region towards Cas A are assumed to be associated-with molecular clouds in that direction.

Warm Gas Models

In the warm gas model we consider $T_e = 75\ K$ which is typical of the temperatures prevailing in neutral H I clouds. The electron density and the radiation temperature are again chosen to be consistent with the observed line width at 34.5 MHz. The three combinations of n_e and T_{R100} considered are 0.16 cm^{-3} and 800 K, 0.12 cm^{-3} and

Table 4.3 Parameters of various models in Figs 4.5, 4.6, 4.7.

T_e K	n_e cm^{-3}	T_{R100} K	EM cm^{-6} pc	S pc	δ_C -	n_H T_e cm^{-3} K
20	0.68	800	0.016	0.03	0.5	9×10^4
	0.49	1600	0.016	0.07	0.5	6.6×10^4
	0.11	3200	0.019	1.6	0.5	1.5×10^4
75	0.16	800	0.018	0.7	0.5	8×10^4
	0.12	1600	0.016	1.11	0.5	3×10^4
	0.03	3200	0.012	13.3	0.5	7500
75	0.101	1600	0.015	1.5	0.5	5×10^4
35	0.05	800	0.004	1.6	0.6	9722

The model temperature and electron density shown in the last two rows of the table correspond to the best-fitting model parameters given by PAE94. T_e =75 K is for Salem-Brocklehurst boundary condition and T_e =35 K is for Gulyaev-Nefedov boundary condition.

1600 K and 0.03 cm^{-3} and 3200 K. In Fig 4.6, the three models are superposed on the observed data and the model parameters are given in Table 4.3. It is clear from Fig 4.6 that the warm gas models axe able to provide much better fit to the data than the cold gas models. The general trend of the data is well accounted for by all the three models. The curves drawn in Fig 4.6 were all obtained by normalizing the emission measure using the data point at 34.5 MHz. If, instead, a least square fit of the model is made to all the observed points (PAE94), then ,it may he possible to obtain even better fit than seen in Fig 4.6.

A visual inspection of Fig 4.6 shows that the higher electron density model (solid line with n_e =0.16 cm^{-3}) gives a slightly better fit to the data than the lower density model (dash-dot line with n_e = 0.03 cm^{-3}). The difference in these models is the radiation temperature. Although the higher density model provides a better fit to the data, the implied thermal pressure in the cloud is at least an order of magnitude higher than the interstellar pressure. As seen in Table 4.2, the thermal pressure (p/k) in this model is 4 x 10^4 cm^{-3} K assuming that the depletion factor for carbon $\delta_C = 1$ (*i.e.* all

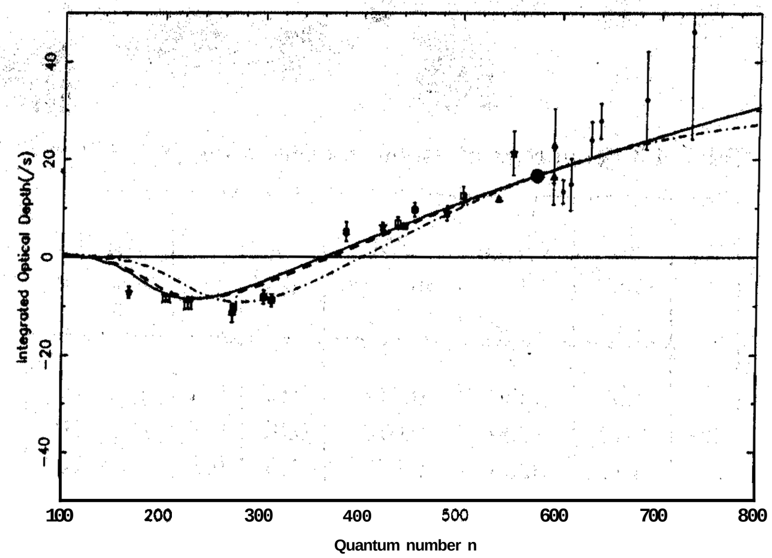

Figure 4.6 Low temperature models - Solid line is for $T_e = 75$ K, $n_e = 0.16$ cm^{-3} & $T_{R100} = 800$ K; the dashed line is for $T_e = 75$ K, $n_e = 0.12$ cm^{-3} & $T_{R100} = 1600$ K; the dash-dotted line is for $T_e = 75$ K, $n_e = 0.03$ cm^{-3} & $T_{R100} = 3200$ K. The influence of dielectronic-like recombination process on the level populations has been included in these models.

the carbon is in gaseous phase). The actual thermal pressure is likely to be a factor of two higher since carbon is known to be depleted on to grains and it is possible that $\delta_C \sim 0.5$.

On the otherhand the thermal pressure in the lower density (n_e =0.03 cm^{-3}) model in Fig 4.6 (dash-dot-dash line) is 7500 cm^{-3} K (assuming $\delta_C = 1$) which is within the range of pressures observed in the ISM. Even if carbon is depleted on to grains with $\delta_C = 0.5$, the derived pressure in this model is within a factor of two of the interstellar value. As seen in Table 4.3, the pathlength through the gas in this low-density model is 13.3 pc, which is comparable to the lateral extent of the gas of > 5 pc and therefore a cloud-like geometry is permissible. In view of these various desirable features, we favour this low-density model for the carbon line region in the direction of Cas A. The parameters of this model are: $T_e = 75$ K, $n_e = 0.03$ cm^{-3}, $T_{R100} = 3200$ K and EM = 0.012 pc cm^{-6}. This model fits the observed variation of line width and line intensity with frequency, predicts a turnover from emission to absorption at about the observed frequency, has an acceptable geometry for the line forming region and implies a thermal pressure in the cloud which is comparable to the pressure in the ISM. On the basis of these physical parameters (especially the temperature and density), we can identify these regions to be coexistent with the neutral H I clouds observed towards

Cas A. This identification is consistent with the result of the previous section in which the spatial distribution of the carbon line region over the face of Cas A was shown to have a good correspondence with the diitribution of optical depth of the 21 cm H I line in this direction. .

4.4 Discussion

In searching for a model that could explain the various observations of low-frequency carbon recombination lines towards Cas A, we arrived above at a model in which the line forming region has $T_e = 75$ K, $n_e = 0.03\ \mathrm{cm}^{-3}$, EM = 0.012 pc cm^{-6} and up to 50 % of carbon may be depleted on to grains. This line forming region is moat likely associated with the neutral H I component in this direction and may be only slightly out of pressure equilibrium with the ISM.

It is actually remarkable that a simple model like this, where the density and temperature are assumed to be uniform, is able to explain most of the observations spanning about two decades in frequency. At the very least, this agreement between the model and the observations tell us that we are on the right track. Further refinements in both model and observations are of course always possible. Our model does not, in fact, give a perfect fit to the observed variation of optical depth with Gequency (see Fig 4.6) and this could be attributed to the simplicity of the model.

A similar model with slightly different parameters has been discussed by PAE94 and they point to two difficulties with such a model. The first problem is that the thermal pressure implied by the model is too high compared to the pressure in the ISM. This problem, although still there, is less severe in the model that we derive above - the thermal pressure is within a factor of two of the ISM value. But more Importantly, it is not clear whether it is really necessary to require that these clouds be in complete pressure equilibrium with the ISM. Recent high angular observations of H I clouds using VLBI and other techniques (Diamond *et. al.* 1989, Frail *et. al.* 1994) have shown that the H i gas in the galaxy has clumpiness on the scale of few tens of AU and that the thermal pressure in such clumps is very much higher than the interstellar pressure. Also high angular resolution H I observations towards Cas A (Bieging *et. al.* 1991) show structures on a variety of scales again implying that the thermal pressures in these region8 may be high. While these are outstanding problems in understanding interstellar H I which need to be pursued, it tells us that pressure equilibrium is not a strict criteria to be applied for modelling the low-frequency recombination lines of carbon. In 'fact, if we relax this criteria, we can get a much better fit to the data in Fig 4.6, while still being consistent with the observed variation of line width with frequency. Such a model is shown in Fig 4.7 and its parameters are listed in Table 4.3.

The second problem with this type of model that was pointed out by PAE94 concerns the thermal balance in the line forming region. PAE94 argue that if the carbon line forming regions are associated with H I clouds, then it is possible to perform calculations to find the equilibrium temperature of the cloud by combining the physical parameters derived from the recombination line data with the results of H I observations at A21 cm. These calculations involve balancing the total heating by cosmic rays, photoelectric emission from grains and by polyaromatic hydrocarbons with cooling by collisional ionization, recombination, collisions with grains and by radiative transitions. Such a calculation was performed by PAE94 and they show that the derived equilibrium temperature is at least a factor of 2 lower than the temperature that fit the recombination line data. These modeb thus fail the thermal balance check.

Faced with these two difficulties (*i.e.* high thermal pressure and low equilibrium temperature), PAE94 considered a new class of models to explain the low-frequency recombination lines of carbon towards Cas A. In these models the departure coefficients b_n and β_n are calculated by taking into account non-ideal plasma effects on high quantum number states such as disruption of the levels by collisions with neutral atoms and electrons (Hummer and Mihalas 1988, Gulyaev and Nefedov 1989). These effects imply that at some large values of the quantum number n, the levels must be empty. This effect is quantified in terms of an "occupation probability", w_n, which is calculated from the physics of the particle interactions. The absence of bound states at high quantum number levels is taken into account by changing the boundary condition for calculating the departure coefficientsto $b_n \to 0$ as $n \to \infty$. These new class of models led PAE94 to a different set of parameters for the carbon line farming regions towards Cas A. The model selected by them is displayed in Fig 4.7 as a dashed curve. The parameters of this model are $T_e = 35$ K, $n_e = 0.05$ cm^{-3}, δ_C −0.6 and $T_{R100} = 800$ K.

The desirable features of the new type of model by PAE94 are that it (1) fits the observed variation of optical depth of the carbon line with frequency reasonably well, (2) is consistent with A21 cm H I absorption measurements in this direction, (3) provides for pressure equilibrium with the ISM and finally (4) passes the thermal balance check based on the heating and cooling rates in atomic clouds. However this model does not explain one of the important observed parameters, namely, the variation of line width with frequency. The fitted parameters of this model (T_e, n_e, and T_{R100}) produce much less line broadening than observed at low frequencies. The variation of line width predicted by their model is shown as a thin solid line in Fig 4.2. PAE94 left the

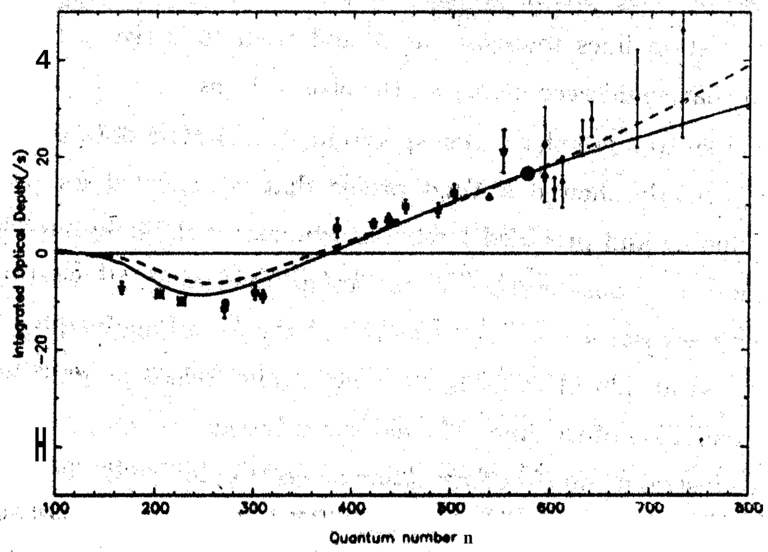

Figure 4.7 The solid line is the best-fitting model with the Salem-Brocklehurst boundary condition for T_e = 75 K, n_e = 0.101 cm^{-3} , T_{R100} = 1600 K. and the dashed line is the best-fitting model with the Gulyaev-Nefedov boundary condition - both these are taken from Payne, Anantharamaiah & Erickson 1994

resolution of this problem to future investigations.

We did not find any solution to this problem through our modelling although we tried a few variations in the computation of the departure coefficients using the modified boundary condition of PAE94. It is clear that non-ideal plasma effects on the population of high quantum number states are important for understanding low-frequency recombination lines and it is necessary to pursue such studies. At this stage, however, given the uncertainties in the calculation of thermal balance (many parameters are involved) and the mounting evidence for high thermal pressures in H I regions, we regard that it is more important for the models to account for the observations than to completely satisfy the requirements of thermal and pressure balance. The model that we derived in the previous section does account for all the observations reasonably well and the parameters of the model suggest that the regions could be in rough pressure equilibrium with the ISM. We did not perform the thermal balance check, but judging from the results of PAE94, the model is likely to predict a temperature which is about a factor of two lower. It is possible that a more refined treatment of the thermal balance calculation may indeed also satisfy this requirement.

4.5 Summary

In this chapter we have presented the interpretation of the various observations of carbon recombination lines towards Cas A and tried to derive a model of the line forming region that could account for all the observations.

The high signal to noise absorption spectrum at 34.5 MHz obtained with the Gauribidanur array clearly showed a Voigt profile that is expected for pressure and/or radiation broadening and provided a reliable estimate of the integrated optical depth at this frequency. On considerations of radiation broadening, a lower limit of 125 pc was derived for the distance between Cas A and the absorbing clouds. The emission spectrum obtained at 328 MHz using the Ooty Radio Telescope gave an estimate of the Doppler broadening of the line. The measured Lorentzian width of the line at 34.5 MHz provided constraints on the combination of electron temperature, electron density and radiation temperature in the line forming region. The parameters suggested that the line forming region could be associated with either molecular (H_2) or atomic (HI) gas in the direction of Cas A.

We then compared the spatial distribution of the C270α line over the face of Cas A, obtained using the Very Large Array, with the distribution of ^{12}CO emission obtained using the 10.4 m millimeter-wave telescope at RRI and also with the distribution of HI optical depth in that direction. The comparison indicated that the carbon line forming region in the direction of Cas A is more likely associated with the atomic HI gas rather than the molecular (H_2) gas.

We combined our data with other available observations towards Cas A in the frequency range 14 MHz to 1400 MHz and explored two types of models, the cold gas model and the warm gas model, to explain the observed variation of line width and line strength over the entire frequency range. In both the models, we considered only the combination of electron temperature, electron density and radiation temperature that were constrained by the observed width of the line at 34.5 MHz. We found that the cold gas model (T_e = 20 K), which implicitly assumes the association of the carbon line region with molecular clouds, does not fit the observations. On the otherhand the warm gas model (T_e = 75 K), provides good fit to the data and thus supports the scenario in which the carbon lines are formed in neutral HI regions in the direction of Cas A. The fitted parameters of the model are: T_e = 75 K, n_e = 0.03 cm^{-3} , T_{R100} = 3200 K, and EM = 0.012 cm^{-6} pc. These parameters imply that the line forming regions are in rough pressure equilibrium in the ISM.

We end the chapter with a discussion of an alternative model presented by PAE94 in which the departure coefficients b_n and β_n were computed after taking into account non-ideal plasma effects on the population of high quantum number states. Although this model has a number of desirable features, it does not account for the observed variation of line width with frequency.